ELSEVIER

Modeling glasses using the reverse Monte Carlo algorithm: Addition of nuclear magnetic resonance and expanded coordination number constraints

J.C. McLaughlin and J.W. Zwanziger

Department of Chemistry, Indiana University, Bloomington, IN 47405, USA

In simple oxide glasses the coordination number and oxidation state of the glass-forming element can be predicted directly from the "8 − n" rule. Tellurite glasses, however, are unusual in that the coordination number of oxygen around tellurium varies without a corresponding change in the oxidation state of tellurium. To model sodium tellurite glasses successfully using the reverse Monte Carlo algorithm several new constraints have been added. Changes include extending the original coordination constraint to allow multiple coordination numbers, and the addition of a new coordination constraint to keep the oxidation state of tellurium constant by limiting the number of bridging and nonbridging oxygens bonded to each tellurium atom. In addition, the second moment of the distribution of dipolar couplings for sodium atoms obtained from a spin-echo NMR experiment was added as a new constraint. The resulting real-space models are presented and the effectiveness of the new constraints is discussed. © 2000 by Elsevier Science Inc.

INTRODUCTION

The reverse Monte Carlo (RMC) algorithm developed by McGreevy and Pusztai[1] has introduced a powerful new tool for developing real-space models consistent with experimental data from multiple experiments. The primary advantage of the algorithm is that any property dependent on the spatial distribution of the atoms within the model can be calculated and thus used as a constraint. This includes structure factors and pair distribution functions from neutron and X-ray diffraction experiments, and also data from EXAFS experiments. In addition, average and absolute coordination constraints between atoms can be stipulated, allowing data from other techniques to be used as constraints on the model.

A wide variety of systems have been explored using the RMC algorithm, including molten salts,[2] amorphous semiconductors,[3] liquid alloys,[4] glasses,[5] and polymers.[6] Many of the typical glass-forming systems have already been explored, including phosphate,[7,8] borate,[9] and silicate[10] glasses. RMC simulations of glasses have examined a number of questions related to the structure of glasses, including the mixed alkali effect,[8] the origin of the first sharp diffraction peak,[9,11] and ionic conduction.[12]

The purpose of this article is to report our extensions of the RMC approach to modeling glasses with more complex structural chemistry than previously considered. We found that the constraints as originally provided in the RMC algorithm were not sufficiently flexible to model glasses with variable coordination numbers, and we also wished to included spin-echo NMR data on distance distributions as a further constraint.

In the following sections we review the basics of the RMC algorithm, including the constraints that are included in the original code. We then discuss the unique characteristics of sodium tellurite glasses and the experimental data that will be used in the RMC simulations. Next, we present the modifications to the RMC code and show the results of RMC simulations on sodium tellurite glasses. We finish by discussing the impact of the modifications on the models and the new information revealed about the structure of sodium tellurite glasses.

Corresponding author: J.W. Zwanziger.

E-mail address: jzwanzig@indiana.edu (J.W. Zwanziger).

Received 14 September 1999; revised 29 October 1999; accepted 29 October 1999.

655 Avenue of the Americas, New York, NY 10010

1093-3263/99/$–see front matter
PII S1093-3263(99)00035-2

THE REVERSE MONTE CARLO ALGORITHM

The RMC algorithm is a variation of the standard Monte Carlo algorithm,[13] in which rather than minimizing the energy of a configuration, the difference between observables calculated from the model and experimentally measured data is minimized. Details of the RMC algorithm can be found elsewhere[1,14,15] and are only summarized here. In a given model, N atoms at the proper number density, ρ_0, are placed in a cell with periodic boundary conditions. Then some observable quantity G, such as the total pair distribution function or total structure factor, is computed and compared point by point with the experimentally derived quantity. The mean square difference χ^2 is then calculated by

$$\chi^2 = \sum_i \frac{1}{\sigma_e^2} (G_{\text{exp}}(r_i) - G_{\text{model}}(r_i))^2 \quad (1)$$

where σ_e^2 is the standard deviation of the experimental data. For each additional experiment, χ^2 is calculated as shown above, and then added together to give χ^2_{total}, which represents the difference between the model and all of the experimental data. A random atom is chosen and moved to produce a new configuration and χ^2_{total} for the new configuration is calculated as described above. The move, and hence the new configuration, is accepted if $\chi^2_{\text{new}} < \chi^2_{\text{original}}$, indicating an improved fit between the model and experiment. If $\chi^2_{\text{original}} < \chi^2_{\text{new}}$ then the move does not improve the fit between the model and the experiment, and the move is accepted with probability

$$p \propto e^{-(1/2)(\chi^2_{\text{original}} - \chi^2_{\text{new}})} \quad (2)$$

A new atom is moved at random and the above process is then iterated until the difference between the model and experimental data (χ^2) reaches an equilibrium value about which it fluctuates. The model is considered complete at this point.

The use of a proper Markov chain in the RMC algorithm ensures, in principle, that it is possible to sample all structures that are consistent with the experimental data.[15] In practice, when an insufficient number of distinct diffraction experiments (e.g., six for a three-component system) is available to distinguish all the partial pair distribution functions, the RMC algorithm often leads to a range of structures that is simply too large and too varied to provide precise structural information. It should be noted that this is not a problem with the RMC algorithm but a problem of not having enough data to decompose the total structure factor completely into its component partials. To limit the range of possible structures, one can add additional constraints to the model.[16] In addition to number density (ρ_0), these constraints include minimum approach distances for atom pairs (R_{min}) and coordination constraints.

The combination of bulk number density and minimum approach distance between atom pairs results in an excluded volume for each atom. If the necessary number of experiments were available these constraints would only speed up the RMC calculation without changing the final result, assuming reasonable minimum approach distances were chosen. However, in the typical case, in which there are not enough experiments available, the minimum approach distance plays an important role in controlling which atom pairs can contribute intensity to certain peaks. Because of the potentially large impact on the structure, the choice of minimum approach distances needs to be made carefully, and should be based as much as possible on experimental information rather than being treated as a free parameter. This may seem like a weakness in the RMC method, but the use of minimum approach constraints is analogous to the normal method of assigning peaks in a diffraction pattern based on knowledge of typical bond lengths and strengths in related materials.

Models at this point often fit the experimental data very well, but closer analysis reveals that the models generally contain many chemically improbable species. The minimum approach constraint discussed above still does not prevent over- and undercoordination when the different atoms are of similar size, leading to overlapping diffraction peaks. The use of coordination constraints then becomes necessary to define better the correct chemistry and higher order correlations thought to be present. Coordination number constraints also provide a powerful method for including additional experimental data from sources other than diffraction experiments. These other sources can include information from crystal structures, chromatography, NMR, and basic chemical knowledge. Coordination number constraints are specified between pairs of atoms and include both a minimum and maximum distance between which to calculate the coordination number, the desired coordination number, the fraction of atoms with the desired coordination number, and a parameter weighting the constraint relative to other constraints and the experimental data. The coordination constraint can either be an absolute constraint or an average coordination number. The use of coordination constraints results in a further decrease in the size of the configuration space sampled, and also restriction to chemically reasonable structures.

The final structures generated by the RMC algorithm should be consistent with all constraints and experimental data used in the simulation, and also represent as limited an area as possible in the configuration space. A final question that is often asked about RMC-generated models is, how unique are they? Theoretically, for a system described by pairwise potentials only, the RMC algorithm should produce a unique result.[17] Realistically, for situations in which there are a limited number of experiments and higher order correlations are present, the resulting models will not be unique. However, it is not the RMC algorithm at fault, it is the data that allow for diversity in the resulting models. This in fact should be treated as an advantage to using the RMC algorithm since it allows sampling of the entire configuration space, resulting in a range of acceptable structures that can be examined.

SODIUM TELLURITE GLASSES

Although the RMC algorithm has been used to model a number of different types of glasses including silicates, borates, and phosphates, the unique chemistry in the tellurite glass system required that a number of modifications be made to the RMC algorithm for successful application.

Sodium tellurite glasses of composition $(Na_2O)_x(TeO_2)_{100-x}$ (where $x = 10$–30%) are made of a glass former, TeO_2, and a modifier, Na_2O. Unlike typical glass formers such as SiO_2, B_2O_3, and P_2O_5, which requires only moderate quench rates to form a glass, TeO_2 is considered a conditional glass former and requires fast quenching to form a glass. However, addition of a small amount of alkali oxide M_2O (where M = Li, Na, K, Rb)

as a modifier leads to a range of glasses that require only moderate quench rates.

To understand what structures might be possible in the glasses we consider first the crystal chemistry of sodium tellurite. In the sodium tellurite system there are three crystal compositions that together with TeO_2 bracket the glass-forming compositions. These are found at $x = 20$, 33, and 50 mol% Na_2O.[18–20] Five different tellurite polyhedra are found in these crystals[21] (Figure 1). The crystal structures reveal that the coordination number of oxygen around tellurium is either 3 or 4 but that there is no change in the tellurium oxidation state. The conventional nomenclature for such polyhedra is Q^n, where the index n gives the number of bridging oxygens bonded to the central atom. In silicates and phosphates this nomenclature is sufficient, because not only the oxidation state but the coordination number in these glasses is fixed as well. For tellurite glasses, we extend this notation to Q^n_m, where the subscript m gives the coordination number. The resulting Q^n_m for each tellurite polyhedra can also be found in Figure 1.

Using the nomenclature established above, we can describe the structures found in the tellurite crystals as follows. Crystalline TeO_2 has two isomorphs, paratellurite[22] (α-form) and tellurite[23] (β-form). Both forms are made up entirely of a fully interconnected network of 4 coordinate tellurium with 4 bridging oxygens each, or in the above notation, Q^4_4 polyhedra. The fully modified 50 mol% Na_2O crystal[20] is entirely composed of Q^0_3 polyhedra, which consist of a tellurium atom connected to 3 nonbridging oxygens, resulting in a completely cleaved network. At the intermediate compositions of 20 and 33 mol% Na_2O the network is only partially cleaved, and consists of a mixture of both 4 and 3 coordinate tellurite polyhedra. The 20 mol% Na_2O crystal[18] still retains the Q^4_4 polyhedra found in pure TeO_2 but in addition has a number of bonds cleaved to form both Q^3_4 and Q^2_3 polyhedra. The 33 mol% Na_2O crystal[19] contains none of the original Q^4_4 polyhedra and the network is composed of Q^3_4 polyhedra terminated by Q^1_3 polyhedra.

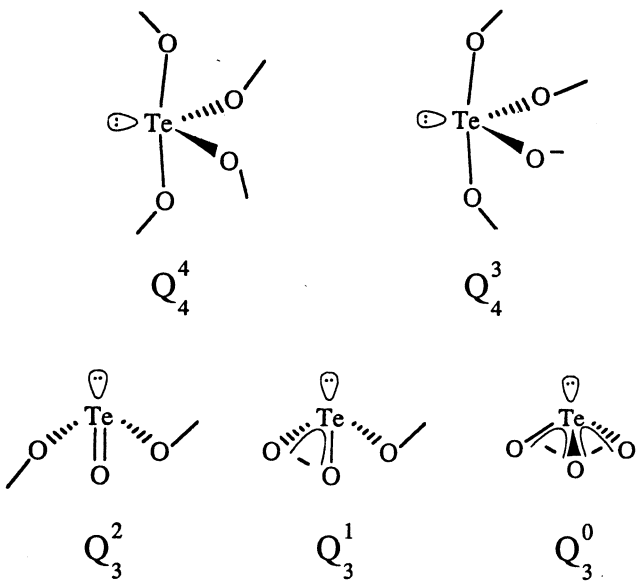

Figure 1. Tellurite structures found in the x = *0.20,* x = *0.33, and* x = *0.50 sodium tellurite crystals. We adopt a terminology in which each structural unit is identified in terms of* Q^n_m, *where* m = *3, 4 and identifies the total number of oxygen bonded to the tellurium atom, and* n = *0, 1, 2, 3 is the number of bridging oxygens bonded to the tellurium atom.*

EXPERIMENTAL METHODS

The $(Na_2O)_x(TeO_2)_{1-x}$ glasses for the NMR, neutron, and X-ray analysis were made by combining appropriate amounts of TeO_2 and Na_2CO_3. Five glasses of composition $x = 12$, 15, 20, 25, and 28 were examined. The mixtures were placed in either a platinum crucible or a silica glass tube and heated at 750°C for 8 min. The molten glass was quenched by pouring between two stainless steel plates, resulting in several thin slabs of glass. The samples were used in the X-ray analysis with no further modification, while for the NMR and neutron analysis the samples were ground into powders. The samples were checked by electron microprobe analysis and determined to be within two percentage points of the calculated composition.

Neutron diffraction experiments were performed at the Intense Pulsed Neutron Source (IPNS), Argonne National Laboratory, on the glass, liquid and amorphous diffractometer (GLAD). The GLAD is a time-of-flight instrument and has been described in detail elsewhere.[24] Samples consisted of approximately 10 g of bulk and crushed glass in a vanadium sample container. For each sample the total static structure factor (Figure 2) was extracted from the measured data using the standard analysis package at the IPNS. The only unusual correction required was a 0.286-Å cutoff of the neutron energy to remove the sharp tellurium neutron absorption resonance at 1.0 eV. Instead of the standard method of Fourier transforming $S(q)$ to obtain $G(r)$ (Figure 2), an inverse method (MCGR) was applied.[25] The MCGR program is similar to the Monte Carlo method developed by Soper[26] and differs mainly in the format of the input and output files. The inverse method was used in order to avoid truncation errors and in order to allow estimation of errors in the $G(r)$ data.

X-ray diffraction experiments were performed at the Advanced Photon Source, Argonne National Laboratory. The measurements were performed on the Sector 1 bend-magnet beam-line (1-BM), operated by the Synchrotron Research and Instrumentation Collaborative Access Team (SRI-CAT). The samples consisted of thin flat plates of glass approximately 0.5 mm thick. An X-ray energy of 61.322 keV was used in order to be well above all absorption resonances. The instrument dead time was measured and corrected for. Following the procedure outlined by Williams,[27] the structure factor $F(q)$ (Figure 2) was extracted from the data by correcting for Compton scattering, absorption, polarization, and background diffraction.

Data from two separate NMR experiments were used in the RMC simulations. Details and results from the experiments have been published previously.[28,29] The first experiment measured the sodium chemical shift, which reveals information about the chemical environment of the sodium cation. The chemical shift can be related empirically to the number of near-neighbor oxygens surrounding each sodium atom.[28,30] The resulting average coordination numbers can be found in Table 1. The second NMR experiment measured the second moment (M_2) of the distribution of sodium–sodium dipolar couplings. The second moment is dependent on both the distance between

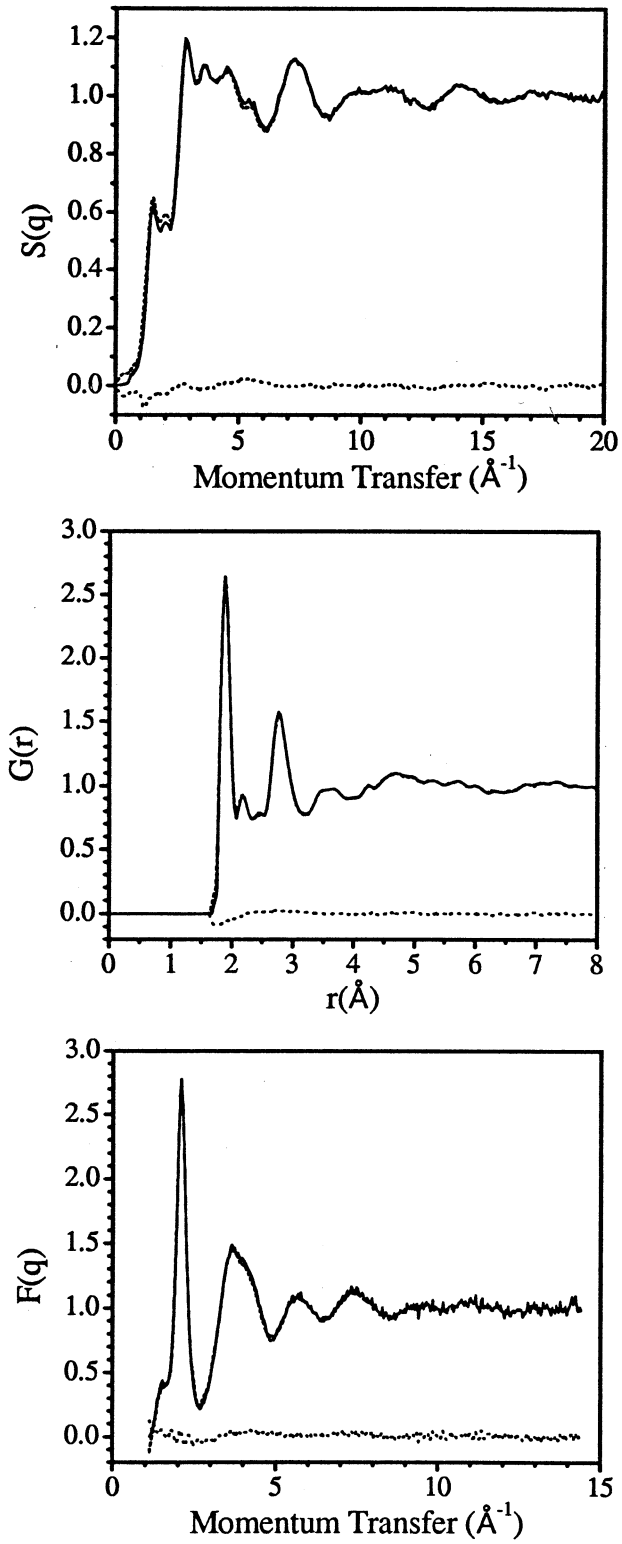

Figure 2. Experimental data (solid curves) and the resulting RMC fit (dashed curves) and residuals (dotted curves) for the $(Na_2O)_{0.2}(TeO_2)_{0.8}$ models. Shown are (a) S(q) *from neutron diffraction; (b)* G(r)*, obtained from* S(q) *by a Monte Carlo-based inversion; and (c)* F(q) *from wide-angle X-ray diffraction (because of the q dependence of the X-ray form factors, these data were not inverted). Data derived from NMR were used simultaneously in the fits, and are listed in Table 1.*

Table 1. Structural Data Derived from NMR Measurements, Used in Construction of Real-Space Models.[a]

mol-% Na_2O	Avg. CN	M_2/C ($\times 10^{-3}$ Å^{-6})
12	5.8	0.75
15	5.8	0.88
20	5.5	3.74
25	5.4	3.95
28	5.4	4.29

[a] The first column gives the sample composition; the second, the average coordination number of oxygen around sodium, as derived from the sodium chemical shift; and the third, the reduced sodium dipolar second moment, as measured in spin-echo decay experiments.

the nuclei and the orientation of the internuclear vector relative to the applied magnetic field. Previously[29] we have related M_2 to the sodium–sodium pair distribution function by

$$M_2 = C_n \frac{9}{5} \sum_j \frac{1}{r_{ij}^6} = C_n \frac{9}{5} \int_0^R \frac{4\pi\rho_0 g(r) r^2}{r^6}\, dr \qquad (3)$$

where C_n is a constant specific to the nucleus probed, ρ_0 is the bulk number density of the nucleus of interest, and the integration is over the sample. The resulting M_2 values used in the RMC algorithm can be found in Table 1.

RMC models were constructed from random starting configurations of 3 750 atoms at the correct number density,[31,32] resulting in models ~40 Å/side. Minimum approach distances were applied for all atom pairs (Table 2) based on distances found in the crystal structures, less about 10% to allow for disorder in bond lengths. Next, the multiple coordination constraints described below were applied. In addition, the average coordination number of oxygen around sodium (Table 1) from NMR was applied. The model were then fit sequentially to $G(r)$ and $S(q)$ from neutron scattering and $F(q)$ from X-ray scattering. Finally, the last two modifications to the RMC algorithm were applied: a constraint to limit the tellurite polyhedra to those Q_m^n species found in the crystals (Figure 1), and a constraint that the sodium–sodium partial $g(r)$ also produce the

Table 2. Closest Approach Distances and Weight Coefficients for the 20 mol-% Composition.

Atom pair	R_{min} (Å)	Neutron weight	X-ray weight ($q = 0$)
Te–Te	3.08	0.079	0.481
Te–Na	3.16	0.049	0.098
Te–O	1.68	0.355	0.327
Na–Na	3.08	0.007	0.005
Na–O	2.16	0.110	0.033
O–O	2.48	0.400	0.056

[a] For each atom pair, the closest approach distance R_{min} used in the RMC models is given. These values are about 10% less than the shortest comparable distances found in sodium tellurite crystals. Given also are the Faber–Ziman weighting coefficients of each atom pair in the total neutron structure factor, and the comparable weights at $q = 0$ in *x*-ray diffraction.

correct second moment (Table 1). In addition to models with all the constraints, models were produced in which one or more constraints were not included in order to explore their effect on the final models.

MODIFICATIONS TO THE RMC PROCEDURE

The standard RMC code was modified in in three ways. First, the original coordination number constraint was extended to include multiple coordination numbers; second, a constraint was added to limit the types of polyhedra; and third, the code was modified to include M_2 [Eq. (3)].

The original coordination number constraint specified both a coordination number and a percentage of atoms that should have the required coordination number. For glasses in the silicate, borate, and phosphate systems the original coordination constraint was sufficient to describe the structure of the basic polyhedra. This is because the coordination of oxygen around silicon and phosphorus is always 4, and in the case of borates ^{11}B NMR can provide good estimates on the proportion of 3- and 4-coordinate boron. For tellurites the Te coordination is one of the key, controversial quantities sought from experiment; it is only clear that both 3- and 4-coordinate species are present, but not the proportion. The solution to this was simply to allow for multiple coordination numbers instead of limiting the constraint to one coordination number. With this new constraint the coordination of oxygen around tellurium was constrained to be 3 or 4 and the coordination of tellurium around oxygen was constrained to be 1 or 2. Both constraints are consistent with the tellurite polyhedra found in the crystal structures.

In addition to allowing multiple coordination numbers to describe the tellurite polyhedra it is also necessary to constrain the number of bridging and nonbridging oxygens attached to each tellurium in order to maintain the correct oxidation state for tellurium. We categorize this as a second neighbor constraint because the identity of the atom(s) attached to the oxygen atoms around a tellurium atom is important. In this case we are concerned with whether the oxygen atoms around a central tellurium atom are bonded to other tellurium atoms (bridging oxygen) or not bonded to any other atom (nonbridging oxygen). Since we use the Q^n_m nomenclature to describe this bonding, and to differentiate the constraint from the normal coordination number constraints we refer to this as a Q^n_m constraint. This constraint was implemented to allow only the five tellurite polyhedra in the crystal structures to be found in the models. No constraint was placed on the proportions of the polyhedra present.

The last modification to the RMC algorithm was the addition of the M_2 constraint. This was simple to add because the RMC algorithm calculates each partial $G(r)$ after every move. It was then only necessary to calculate the M_2 integral in Eq. (3) and compare it with the experimental value. The constraint was weighted in the same way as the other constraints.

RESULTS

Results are presented showing the effectiveness and unique information that can be obtained from the new constraints added to the RMC algorithm. The resulting real-space models were consistent with the experimental data as shown in Figure 2. The addition of the Q^n_m constraint led to models containing only those tellurite species found in the crystals as shown in Figure 3 for the 20 mol% Na_2O glass. The distribution of acceptable tellurite polyhedra was not constrained, and the resulting Q^n_m distribution as a function of mol% Na_2O is shown in Figure 4. The M_2 and sodium–sodium partial $G(r)$ for three models can found in Figures 5 and 6.

DISCUSSION

The real-space models generated show excellent agreement with the experimental data (Figure 2), indicating that the minimum contact distances and coordination constraints applied do not conflict with the actual experimental data. One should note that this does not indicate that the constraints are correct, or that other constraints would be incorrect, only that the constraints used are consistent with all of the experimental data.

Q^n_m Constraint

Without application of the Q^n_m constraint many chemically improbable species can be generated by the RMC algorithm since insufficient information about higher order correlation functions is contained in the experimental data. Examination of Figure 3 shows the distribution of tellurite polyhedra for the 20 mol% Na_2O glass models with and without the Q^n_m constraint. The total percentage of unacceptable species was 33.9% in the model without the Q^n_m constraint and only 3.9% for the model with the Q^n_m constraint. The Q^n_m constraint was quite effective in removing unwanted tellurite species without significantly decreasing the level of agreement with the experimental data,

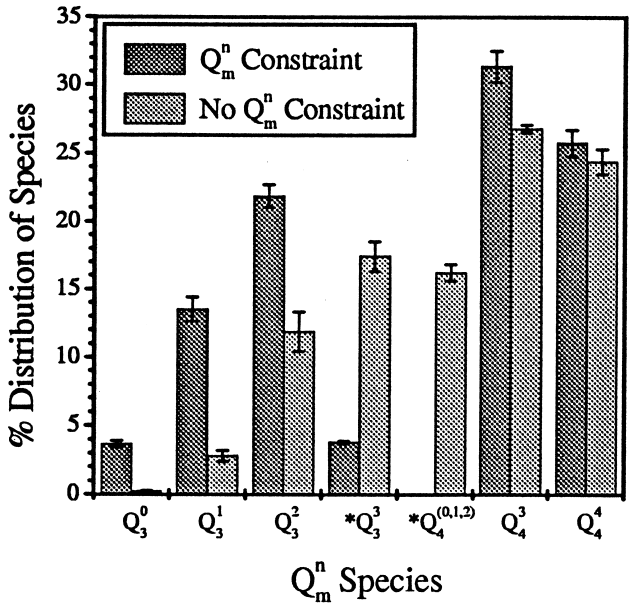

Figure 3. Distribution of tellurite species with and without the Q^n_m *constraint. All other constraints (*R_{min}*, Te and O coordination numbers) and experimental data [*S(q), G(r), F(q)*, average Na–O coordination number, and* M_2*] were the same. Tellurite species not found in the crystals are marked with an asterisk (*).*

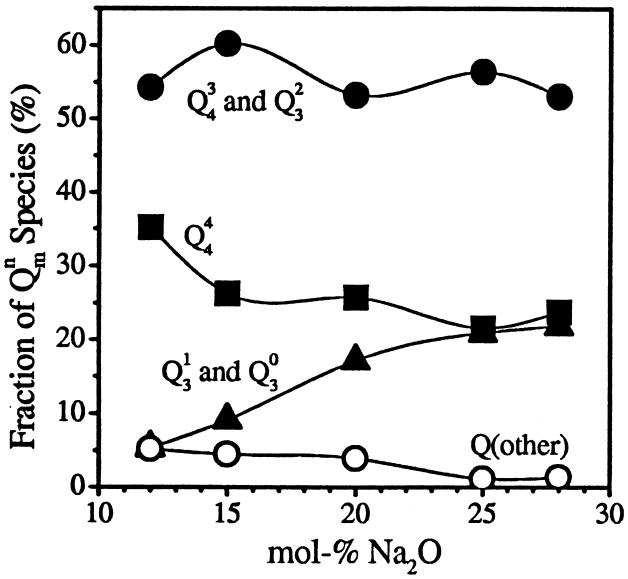

Figure 4. Proportion of the Q^n_m species found in the models. (■) Q^4_4; (●) Q^3_4 and Q^2_3; (▲) Q^1_3 and Q^0_3; (○) other Q^n_m species.

although an increase in computation time was necessary. Including the constraint and still being able to fit the experimental data indicates that the expectation of finding similar structures in the crystals and glasses is not unrealistic.

One can monitor the modification of the tellurite glass as a function of added Na_2O by monitoring the change in the

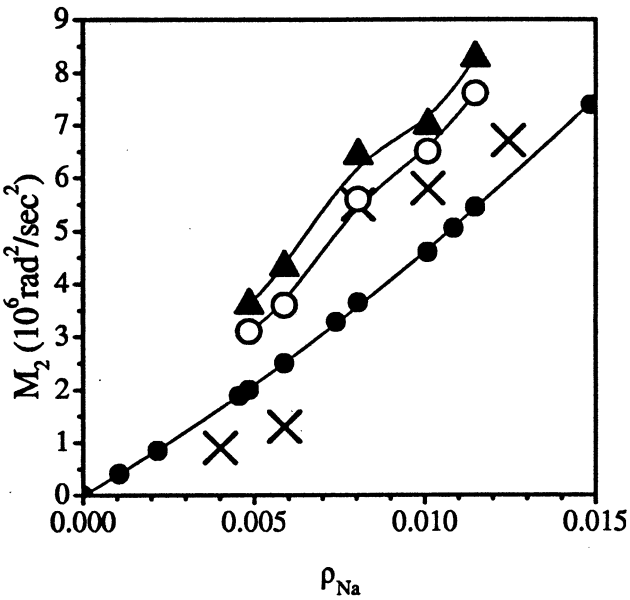

Figure 5. Experimental and model sodium second moments, M_2. (×) Experimental values; (●) model 1; (○) model 2; and (▲) model 3. The M_2 values for model 4 correctly reproduced the experimental M_2 values and therefore are not plotted. The line for model 1 is the best fit line to a cubic polynomial, while the other lines are provided as guides to the eye, and do not represent fits to the model data.

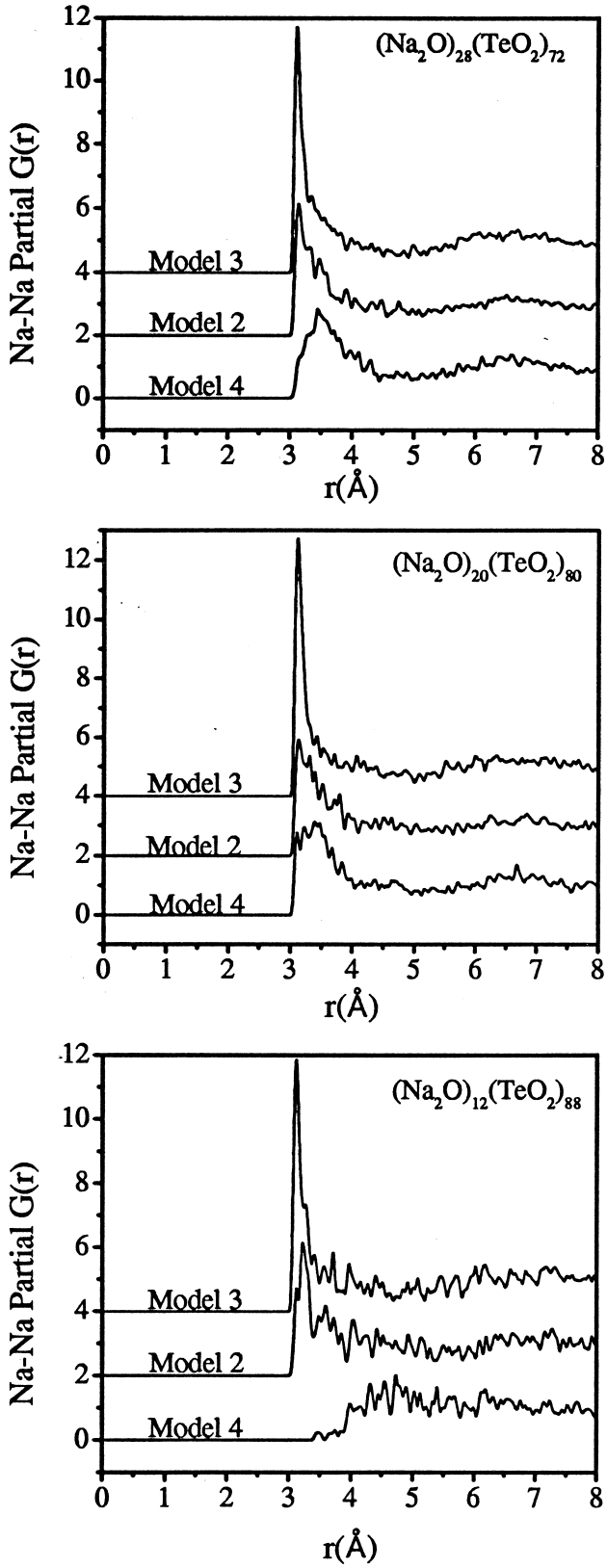

Figure 6. The sodium–sodium pair distribution function from the RMC models for the 12, 20, and 28 mol% Na_2O glass compositions. Results from three models are shown. Solid line, model 2; dashed line, model 3; dotted line, model 4.

distribution of Q_m^n species as shown in Figure 4. Several general trends are apparent as the modification proceeds. As the mol% Na_2O increases, the Q_4^4 polyhedra, which made up the fully connected network in TeO_2, decrease steadily from about 35 to 20% of the total Q_m^n polyhedra. Taken together, the Q_4^3 and Q_3^2 groups, which maintain the majority of the network connectivity while still possessing one nonbridging oxygen, are constant at about 55%. The Q_3^1 and Q_3^0 groups increase steadily from about 5 to 20%, indicating the breaking up of the TeO_2 network, as they result in the formation of a terminating group or a lone TeO_3^{2-} group respectively. Overall, it appears that the breakup of the original TeO_2 network occurs gradually as a function of added modifier.

These results agree qualitatively with earlier neutron diffraction and Raman scattering experiments but yield much more quantitative information. In an early neutron diffraction experiment, Neov et al.[33] examined a 20 mol% Li_2O glass for which a coordination number for oxygen around tellurium of ~4 was measured. This was interpreted as being due to the conversion of Q_4^4 groups in pure TeO_2 to Q_4^3 groups. By simulating $G(r)$ using this mechanism they concluded that 40% of the Q_4^4 groups undergo this conversion. This differs somewhat from the RMC simulation of the 20 mol% Na_2O glass, where a coordination number of 3.6 ± 0.1 and a distribution of ~27% Q_4^4, ~32% Q_4^3, and ~40% Q_3^n groups was found. This seems to indicate that in the sodium tellurite glasses the breakup of the network is more extensive and varied than that suggested by Neov et al.

Raman scattering experiments by Sekiya et al.[34] on Na_2O and Tatsumisago et al.[35] on Li_2O modified tellurite glasses both made several qualitative predictions on the types of units present in the glasses. They predict the existence of all the Q_m^n groups found in the crystals, except for the Q_3^0 group, which occurs only in the 50% crystal, well outside the normal glass-forming region. One should note that these predictions were made before the 20 and 33% crystal structures were solved. No quantitative predictions were given for the distribution of Q_m^n species. This appears to agree well with our results except for the small fraction (0.5 to 6%) of Q_3^0 groups that the RMC models predict.

With the exception of the Q_3^0 groups, present at only a small concentration, all other Q_m^n species found in crystals were necessary to obtain a good fit to the data. We examined in particular the model proposed by Sakida and co-workers, in which Q_3^2 groups are explicitly excluded on the basis of calculations of Raman transitions.[36] We found that if such groups are excluded, the models do not fit even a limited amount of the diffraction data. We would thus reject with confidence the model proposed. Such questions are ideal for the RMC method: Given a plausible set of polyhedra, can any one be excluded and still obtain a model consistent with the diffraction data? Inclusion of second-neighbor Q_m^n constraints makes this type of question particularly easy to address.

M_2 Constraint

Next, the effect of the M_2 constraint on the models was explored. Previous to obtaining the neutron and X-ray diffraction data presented here, we attempted to model various distributions of the sodium ions without including any information about the TeO_2 network.[29] All models tried fit into one of two categories[29]: models that increased linearly with the sodium number density, and models that increased quadratically with ρ_{Na}. None of these simple models could fit the large increase in M_2 at approximately 20 mol% Na_2O that is seen in the experimental data.

While no single model has proven sufficient to describe the sodium ion distribution, a series of different models (see Table 3 and Figure 5) have provided some insight into the sodium ion distribution. In the article mentioned above[29] we reported results for a hard sphere model of sodium atoms, which we will refer to here as model 1. The only constraints to this model are the sodium number density, and a minimum approach distance between the sodium atoms of 3.08 Å based on sodium–sodium distances found in the crystal structures. The simple hard sphere model fails to capture the large increase in M_2 at the 20 mol% Na_2O composition, but it does provide a starting point for examining the sodium atom distribution, as model 1 represents a random distribution of the sodium atoms. In the density regime studied here, the resulting M_2 values can be fit to a cubic polynomial quite well, as shown in Figure 5.

In model 2, more information was added by including the Te and O atoms into the hard sphere model and constraining it using the minimum approach distances in Table 2. The inclusion of Te and O atoms into the hard sphere model more realistically represents the random distribution of sodium atoms in a tellurite network, although no information about the structure of the network has been included yet. The simple hard sphere potential in the previous model is now directly modified by the addition of interactions between Na–Te and Na–O and is also modified indirectly by the interactions between Te–Te, Te–O, and O–O. The resulting effective potential is compli-

Table 3. Constraints Used in Generating Each Model[a]

Model	Atoms	Coordination Number (Te and O)	Average Coordination Number (Na–O)	Diffraction data		
				$S(q)$, $G(r)$, $F(q)$	Q_m^n	M_2 (Na)
1	Na					
2	Na, Te, O	√	√			
3	Na, Te, O	√	√	√	√	
4	Na, Te, O	√	√	√	√	√

[a] An *x* indicates that the constraint was applied. The R_{min} constraint was used in all models. Coordination number constraints for Te and O were derived from the crystal structures. The coordination of Te was required to be 3 or 4 and for oxygen 1 or 2. The values for the average coordination number for oxygen around sodium and M_2 for sodium were determined from NMR experiments and are given in Table 1.

cated and difficult to picture, but the resulting trend in M_2 does begin to show a small step at ~20 mol% Na_2O. The resulting M_2 is also higher than both the experimental and model 1 M_2 values, indicating that the sodium atoms are closer together on average than in the simple hard sphere model or in the glass. This is probably due to the decreased volume available to the sodium atoms because of the presence of the Te and O. While model 2 shows a small step, overall it fails to capture the large increase in M_2 at the 20 mol% Na_2O composition.

Model 3 includes the addition of the Q_m^n constraint and the experimental diffraction data in order to model the tellurite network correctly. While the diffraction data do include a small amount of information about the sodium–sodium distribution, we recall from Table 2 that this is small compared with the information about the tellurite network. The resulting M_2 values are higher than those in model 2, and the step at ~20 mol% Na_2O composition is slightly more prominent. The increase in M_2 is due to an increase in the number of sodium atoms at the closest approach distance. This can be clearly seen in Figure 6, which shows a plot of the Na–Na partial $G(r)$ for models 2–4 for the 12, 20, and 28 mol% Na_2O glasses. The increase in M_2 over model 2 is probably due to a further decrease in the volume available to the sodium atoms because of the additional constraints. In addition, the experimental data change the distribution and interactions between the Te–O, Te–Te, and O–O atoms considerably, changing the effective potential felt by the sodium atoms. Model 3, then, should represent the most realistic model for a random distribution of sodium atoms within the tellurite network.

In model 4 we finally add the M_2 constraint. The resulting models have the correct M_2, without noticeably worsening the fit to the other constraints. Table 2 shows that the diffraction experiments contain little information about the Na–Na interactions, therefore the M_2 constraint combined with the R_{min} constraint is playing the major role in controlling the distribution of sodium atoms in the model. While giving a large change in M_2 from model 3, neither the coordination numbers (with the obvious exception of the Na–Na coordination number) or the Q_m^n distributions show a large change. Apparently the sodium–sodium distribution and the TeO_2 network are not strongly linked. This agrees well with previous observations that the bulk properties in tellurite glasses, including molar volume, glass transition temperature, and thermal expansion coefficients, change almost linearly with increasing modifier content, instead of abruptly as the sodium distribution appears to.

More can be learned about the distribution of sodium ions in tellurite glasses by comparing the Na–Na partial $G(r)$ values from several of the models. As noted earlier, the intensity of the maximum in $G(r)$ increases for all glass compositions between models 2 and 3, indicating that on average more sodium ions are found at the minimum Na–Na contact distance. Model 4 shows the opposite effect, with intensity at the minimum approach distance decreasing because the M_2 constraint is forcing the sodium atoms further apart. This is most pronounced for the 12 and 15 mol% Na_2O models, where the sodium density does not reach a maximum until ~4.5 Å. For the 20 mol% Na_2O models the partial $G(r)$ looks much the same for models 2 and 4 because the M_2 values for both models are nearly the same. For the 25 and 28 mol% Na_2O models the $G(r)$ from model 4 shows a shift in the intensity of the peak from R_{min} to larger r because the M_2 is required to decrease in model 4 from the values observed in models 2 or 3. From our construction of models 2 and 3 we know that the sodium atoms are randomly distributed in the tellurite network. We can then conclude from the sodium–sodium partial $G(r)$ values of model 4 that, when compared with the hard sphere like distributions of models 2 and 3, the sodium atoms should have a larger sodium–sodium minimum approach distance. This is most noticeable in the 12 and 15 mol% Na_2O models, and less so in the 20, 25, and 28 mol% Na_2O models. This difference might indicate that different R_{min} values should be used at different compositions. While it is possible to model the glasses using a larger sodium–sodium minimum approach distance, and varying the distance with composition, the number of models that can be produced in this matter is problematic and likely contains little additional information. The origin of the step seen in the experimental data appears, after examining models 2 and 3, to be a function of order in the tellurite network and not in the sodium atom distribution.

Although a unique model cannot be derived to describe the sodium atom distribution, we can comment on what types of distributions are not supported by the RMC models and the experimental data. This is important because several models for ion diffusion and conductivity in glasses predict different cation distributions in the glasses. One such model is the modified random network (MRN),[37,38] which predicts that the modifier cations are found clustered in regions or channels in the glass. The most obvious place to look for clustering is in the Na–Na pair distribution function (Figure 6). The first coordination shell of sodium is composed of oxygen atoms, leaving the second shell, roughly between 3 and 4 Å, composed of either tellurium or sodium atoms. On examining the Na–Na pair distribution function for the 12 and 15 mol% Na_2 models it is clear that almost no sodium atoms are found in the second coordination shell. This argues strongly against clustering in the glasses at low modification. For the 20, 25, and 28 mol% Na_2O models there is significant sodium density between 3 and 4 Å. In comparing model 4 with models 2 and 3 we see a noticeable shift in the sodium density away from R_{min}, to slightly larger distances, occurring as the sodium density increases. This argues against sodium atom clustering in these models although it is not as clear as at low modification. A slightly larger R_{min} distance for Na–Na would perhaps erase this shift; however, there is certainly no extra intensity at R_{min} compared with the pure hard sphere models, which would be a clear sign of clustering. In all cases the shift in sodium density to larger distances is compensated for by the shifting of tellurium density to shorter distances, indicating that tellurium is favored over sodium in the second coordination shell. The Na–Na and Na–Te average coordination numbers also show no indication of Na–Na clustering. Thus, we conclude that the sodium atom distribution in the glasses most closely fits a random model, and is not consistent with excess clustering.

CONCLUSIONS

Through the use of the RMC algorithm to combine multiple sets of experimental data, and the addition of the Q_m^n and the M_2 constraint, we are able to obtain additional information about the structure of tellurite glasses that is unavailable from a direct analysis of the experimental data. Information about the distribution of tellurite polyhedra indicates the presence of all tellurite polyhedra found in the crystals and shows the gradual breakup of the TeO_2 network. By combining NMR data and

diffraction data, and using a variety of different constraints to generate a series of models, we have also concluded that the sodium atom distribution appears to be random, with a minimum approach distance larger than 3.08 Å, which probably varies with composition. The RMC algorithm, used carefully to generate models consistent with the experimental data, is a powerful tool for generating insights into the structure of glasses and other disordered materials.

ACKNOWLEDGMENTS

This work was supported by the NSF under Grants DMR-9508625 and DMR-9870246, and was discussed in part at the 1998 National Meeting of the American Crystallographic Association, in conjunction with the Workshop on Modeling Disordered Materials. We gratefully acknowledge experimental assistance from Dr. Dean Haeffner and Dr. Sarvjit Shastri at the APS, and from Dr. Yaspal Badyal and Dr. Jackie Johnson at the IPNS.

REFERENCES

1. McGreevy, R.L., and Pusztai, L. Reverse Monte Carlo simulation: A new technique for the determination of disordered structures. *Mol. Simul.* 1988, **1,** 359–367
2. McGreevy, R.L., and Pusztai, L. The structure of molten salts. *Proc. R. Soc. Lond. A.* 1990, **430,** 241–261
3. Gereben, O., and Pusztai, L. Structure of amorphous semiconductors: Reverse Monte Carlo studies of a-C, a-Si, a-Ge. *Phys. Rev. B* 1994, **50,** 14136–14143
4. Pusztai, L. Partial pair correlation functions of some Ge-Sb liquid alloys from single diffraction measurements. *ACH Models Chem.* 1995, **132,** 99–110
5. Wicks, J.D., Börjesson, L., Bushnell-Wye, G., Howells, W.S., and McGreevy, R.L. Structure and ionic conduction in $(AgI)_x(AgPO_3)_{1-x}$ glasses. *Phys. Rev. Lett.* 1995, **74,** 726–729
6. Carlsson, P., Swenson, J., Börjesson, L., Torell, L.M., McGreevy, R.L., and Howells, W.S. Structural properties of poly(propylene oxide) from diffraction experiments and reverse Monte Carlo simulation. *J. Chem. Phys.* 1998, **109,** 8719–8728
7. Wicks, J.D., Börjesson, L., Bushnell-Wye, G., Howells, W.S., and McGreevy, R.L. Modelling the structure and ionic conduction of $(AgI)_x(AgPO_3)_{1-x}$) glasses. *Phys. Scripta* 1995 **T57,** 127–132
8. Wicks, J.D. Studies of Disordered Materials. Ph.D. thesis, Oxford University, Oxford, U.K., 1993
9. Swenson, J., and Börjesson, L. Intermediate range order in a network glass. *J. NonCrystalline Solids* 1998, **223,** 223–229
10. Uhlig, H., Hoffmann, M., Lamparter, H., Aldinger, F., Bellissent, R., and Steeb, S. Short-range and medium-range order in lithium silicate glasses. II. Simulation of the structure by the reverse Monte Carlo method. *J. Am. Ceram. Soc.* 1996, **79,** 2839–2846
11. Swenson, J., Börjesson, L., McGreevy, R.L., and Howells, W. Structure of $AgI\text{-}Ag_2O\text{-}2B_2O_3$ glasses: A neutron and X-ray diffraction investigation. *Phys. Rev. B* 1997, **55,** 11236–11248
12. Swenson, J., McGreevy, R.L., Börjesson, L., and Wicks, J. Relations between structure and conductivity in fast ion conducting glasses. *Solid State Ionics* 1998, **105,** 55–56
13. Metropolis, N., Rosenbluth, A.W., Rosenbluth, M.N., Teller, A.H., and Teller, E. Equation of state calculations by fast computing machines *J. Chem. Phys.* 1953, **21,** 1087–1092
14. McGreevy, R.L., and Howe, M.A. RMC: Modeling disordered structures. *Annu. Rev. Mater. Sci.* 1992, **22,** 217–242
15. McGreevy, R.L. RMC: Progress, problems and prospects. *Nucl. Instr. Methods Phys. Res. A* 1995, **354,** 1–16
16. Pusztai, L. Reverse Monte Carlo simulations for determining disordered structures. In: *Amorphous Insulators and Semiconductors*, Vol. 23 of *NATO ASI Series 3: High Technology* (Thorpe, M.F., and Mitkova, M.I., eds.). Kluwer Academic Publishers, Dordrecht, 1997
17. Evans, R. Some remarks on the reverse Monte Carlo simulation. *Mol. Simul.* 1990, **4,** 409
18. Tagg, S.L., Huffman, J.C., and Zwanziger, J.W. Crystal structure and sodium environments in sodium tetratellurite, $Na_2Te_4O_9$, and sodium tellurite, Na_2TeO_3, by X-ray crystallography and sodium-23 NMR. *Chem. Mater.* 1994, **6,** 1884–1889
19. Tagg, S.L., Huffman, J.C., and Zwanziger, J.W. Crystal structure of sodium ditellurite, $Na_4Te_4O_{10}$. *Acta Chem. Scand.* 1997, **51,** 118–120
20. Masse, R., Guitel, J.C., and Tordjman, I. Preparation chimique et structure cristalline des tellurites de sodium d'argent: Na_2TeO_3, Ag_2TeO_3. *Mater. Res. Bull.* 1980, **15,** 431–436
21. Becker, C.R., Tagg, S.L., Huffman, J.C., and Zwanziger, J.W. Crystal structure of potassium tetratellurite, $K_2Te_4O_9$, and potassium ditellurite, $K_2Te_2O_5$, and structural trends in solid alkali tellurites. *Inorg. Chem.* 1997, **36,** 5559–5564
22. Lindqvist, O. Refinement of the structure of α-TeO_2. *Acta Chem. Scand.* 1968, **22,** 977–982
23. Beyer, H. Verfeinerung der kristallstruktur von tellurit, dem rhombischen TeO_2. *Z. Kristallogr.* 1967, **124,** 228–237
24. Ellison, A.J.G., Crawford, R.K., Montague, D.G., Volin, K.J., and Price, D.L. The new glass, liquids and amorphous materials diffractometer (GLAD) at IPNS. *J. Neutron Res.* 1993, **1,** 61–70
25. Pusztai, L. and McGreevy, R.L. MCGR: An inverse method for deriving the pair correlation function from the structure factor. *Phys. B* 1997, **234,** 357–358
26. Soper, A.K. *An Amateur's Guide to the Pitfalls of Maximum Entropy*. Institute of Physics, Bristol, UK, 1990
27. Williams, A. X-Ray Diffraction Studies of Metallic Glasses. Ph.D. thesis, California Institute of Technology, Pasadena, California, 1980
28. Tagg, S.L., Youngman, R.E., and Zwanziger, J.W. The structure of sodium tellurite glasses: Sodium cation environments from sodium-23 NMR. *J. Phys. Chem.* 1995, **99,** 5111–5116
29. Zwanziger, J.W., McLaughlin, J.C., and Tagg, S.L. The distribution of sodium in sodium tellurite glasses, probed with spin echo NMR. *Phys. Rev. B* 1997, **56,** 5243–5249
30. Koller, H., Engelhardt, G., Kentgens, A.P.M., and Sauer, J. ^{23}Na NMR spectroscopy of solids: Interpretation of quadrupole interaction parameters and chemical shifts. *J. Phys. Chem.* 1994, **98,** 1544–1551
31. Mochida, N., Takahashi, K., Nakata, K., and Shibusawa, S. Properties and structure of the binary tellurite

glasses containing mono- and divalent cations. *Yogyo-Kyokai-Shi* 1978, **86,** 316–326
32. Heo, J., Lam, D., Sigel, G., Mendoza, E., and Hensley, D. Spectroscopic analysis of the structure and properties of alkali tellurite glasses. *J. Am. Ceram. Soc.* 1992, **75,** 277–281
33. Neov, V.K., Gerasimova, I., Krezhov, K., and Sidzhimov, B. A model for structural recombination in tellurite glasses. *J. Phys. C: Solid State Phys.* 1979, **12,** 2475–2485
34. Sekiya, T., Mochida, N., Ohtsuka, A., and Tonokawa, M. Raman spectra of $MO_{1/2}$-TeO_2 (M = Li, Na, K, Rb, Cs, and Tl) glasses. *J. Non-Crystalline Solids* 1992, **144,** 128–144
35. Tatsumisago, M., Minami, T., Kowada, Y., and Adachi, H. Structural change of rapidly quenched binary tellurite glasses with composition and temperature. *Phys. Chem. Glasses* 1994, **35,** 89–97
36. Sakida, S., Hayakawa, S., and Yoko, T. Part 2. ^{125}Te NMR study of M_2O-TeO_2 (M = Li, Na, K, Rb and Cs) glasses. *J. Non-Crystalline Solids* 1999, **243,** 13–25
37. Greaves, G.N., Fontaine, A., Lagarde, P., Raoux, D., and Gurman, S.J. Local structure of silicate glasses. *Nature (London)* 1981, **293,** 611–616
38. Greaves, G.N. EXAFS and the structure of glass. *J. Non-Crystalline Solids* 1985, **71,** 203–217